# Biscarbazolylmethane-based cyanine: A two-photon excited fluorescent probe for DNA and selective cell imaging

**ARTICLE** · MARCH 2014

DOI: 10.1039/C3TB21860K



**5 AUTHORS**, INCLUDING:

Mei-Ling Zheng
Technical Institute of Physics and Chemistry
**54** PUBLICATIONS **293** CITATIONS
SEE PROFILE

Shu Chen
Technical Institute of Physics and Chemistry
**4** PUBLICATIONS **27** CITATIONS
SEE PROFILE

Zhensheng Zhao
Technical Institute of Physics and Chemistry
**51** PUBLICATIONS **384** CITATIONS
SEE PROFILE

Journal of Materials Chemistry B



PAPER

View Article Online
View Journal | View Issue



Cite this: J. Mater. Chem. B, 2014, 2, 2301

# Biscarbazolylmethane-based cyanine: a two-photon excited fluorescent probe for DNA and selective cell imaging†

Yong-Chao Zheng,[ac] Mei-Ling Zheng,*[a] Shu Chen,[ac] Zhen-Sheng Zhao[a] and Xuan-Ming Duan*[ab]

Received 30th December 2013
Accepted 6th February 2014

DOI: 10.1039/c3tb21860k

www.rsc.org/MaterialsB

Here, we have introduced a novel biscarbazolylmethane-based cyanine as a two-photon excited fluorescent probe, 6,6′-bis[2-(1-methylpyridinium)vinyl]-bis(9-methyl-carbazol-3-yl)methane diiodide, which has two vinylpyridinium carbazole moieties connected by a non-rigid methylene bridge. This molecule possesses a larger Stokes shift and enhanced two-photon absorption cross-section than the previously reported vinylpyridinium carbazole monocyanine, which is mainly attributed to the "through-space" type intramolecular charge transfer. The low fluorescence quantum yield and 30-fold fluorescence enhancement once binding with calf thymus DNA highlight this molecule as a promising fluorescence light-up probe for DNA. The obvious induced circular dichroism signals have proved that the molecule with soft-connected bis-cationic centers can specifically interact with various DNA structures. Cell viability study shows that the probe has very low cytotoxicity. The probe exhibits high staining selectivity for mitochondria in living HeLa cells. Its capability to stain nuclear DNA has been confirmed by fixed cell staining. Furthermore, the application for two-photon excited fluorescence imaging demonstrates high potential of the probe for nonlinear bioimaging with 3D resolution.

## Introduction

Fluorescent probes, as powerful bioanalytical tools, have played key roles in the fields of bioimaging, disease diagnosis and therapy.[1,2] Two-photon absorption (TPA) has attracted a considerable amount of attention in micro/nanofabrication,[3] optical power limiting,[4] photodynamic therapy[5] and bioimaging.[6] In the past decade, extensive research has been focused on developing novel probes for two-photon excited fluorescence (TPEF) microscopy imaging, which is more practically useful for non-invasive live cell imaging due to deep penetration, low photobleaching and high spatial resolution.[7,8]

Several kinds of probes have been developed, such as small molecular probes,[9,10] analogs of biomolecules,[11] quantum dots[12,13] and nanoparticles.[14,15] The organic fluorescent probe, which is easily modified, probably contributes to the significant fluorescence enhancement once specifically binding to biomolecules. This kind of active light-up type probe has a much higher signal/noise ($S/N$) ratio and is able to improve the imaging sensitivity and specificity *in vivo* in contrast to the traditional fluorophores.[16]

Nucleic acid is the key biomacromolecule in inheritance and reproduction of life.[17,18] In recent years, the probes of DNA have been extensively studied,[19–21] of which the fluorescence intensity can be significantly enhanced when they are intercalated between two base pairs or bound to the minor grooves of the DNA chain.[22,23] Among them, the carbazole scaffold with fused aromatics has recently attracted intense interest because of its biologically active properties.[24] To date, a variety of carbazole derivatives from various natural or synthetic sources have been used as fluorescent probes and antitumor drugs.[25–27] Carbazole-based cyanines are highly sensitive and efficient light-up fluorescent probes for DNA due to their good water solubility, biocompatibility and hypotoxicity,[28] which enable them to stain living tissues and cells.[29]

Stilbazolium-substituted carbazole cores have been commonly employed as specific fluorescent labels for DNA and subcellular structures. Feng *et al.* and Chang *et al.* developed bisvinylpyridinium carbazole derivatives as sensitive probes for

[a]*Laboratory of Organic NanoPhotonics and Key Laboratory of Functional Crystals and Laser Technology, Technical Institute of Physics and Chemistry, Chinese Academy of Sciences, No. 29 Zhongguancun East Road, Beijing 100190, P. R. China. E-mail: zhengmeiling@mail.ipc.ac.cn; xmduan@mail.ipc.ac.cn; Fax: +86-10-82543597; Tel: +86-10-82543596*

[b]*Chongqing Institute of Green and Intelligent Technology, Chinese Academy of Sciences, No. 266 Fangzheng Ave, Shuitu technology development zone, Beibei District, Chongqing 400714, P. R. China*

[c]*University of Chinese Academy of Sciences, No. 29 Zhongguancun East Road, Beijing 100190, P. R. China*

† Electronic supplementary information (ESI) available: Quadratic dependence of TPA and TPEF spectra, absorption and OPEF spectra in buffer and glycol, CD spectra of oligonucleotides, CD titration spectra of probes **II** and **III**, staining dynamics analysis of the probes, co-localization with MitoTracker Deep Red, NMR and ESI-MS spectra of molecules. See DOI: 10.1039/c3tb21860k

dsDNA and G-quadruplex considering their high binding affinity to DNA.[28,30] The binding preference of such derivatives with various DNA secondary structures has been further evaluated.[31] Additionally, several vinylpyridinium carbazole derivatives with a one-dimensional (1D) monocyanine or two-dimensional (2D) biscyanine structure, such as 3-[2-(1-methylpyridinium)vinyl]-9-methyl-carbazoletosylate and 3,6-bis[2-(1-methylpyridinium) vinyl]-9-methyl-carbazole ditosyl-ate, have also been used in TPEF imaging for staining DNA-riched subcellular structures considering their large TPA cross-sections.[29] In previous work, we focused our efforts on the physical properties and the application of vinylpyridinium carbazole cyanines as TPEF probes.[29,32] The molecular structures engineered the specific labels of the nucleus and mitochondria in living cells. These 1D and 2D cyanines exhibit quite different optical properties and biological characteristics.[32] The 1D monocyanine molecule has a $C_v$ symmetric structure containing a donor (D) group and an acceptor (A) group linked by a $\pi$ conjugated system (D–$\pi$–A), while 2D $C_{2v}$ symmetric biscyanine possesses an A–$\pi$–D–$\pi$–A structure. The $C_{2v}$ molecule with 2D intramolecular charge transfer (ICT) is more likely to realize high TPA properties than that of the corresponding 1D compound.[33] Unfortunately, the larger conjugated system of the $C_{2v}$ molecule compared to the $C_v$ molecule leads to the decrease of the Stokes shift, which is unfavourable for a probe to be applied in fluorescence microscopy. However, biscyanines tend to exhibit stronger binding strength to DNA due to their symmetric structures and bis-cationic centres.[34]

Given that the carbazole core in traditional biscyanines is a rigid structure, we are wondering whether a symmetric two-branched cyanine with two vinylpyridinium groups linked by a non-rigid bridge would exhibit a large Stokes shift, large TPA cross-section and high affinity to DNA. In this paper, we have designed a novel biscarbazole-based cyanine TPEF probe, 6,6′-bis[2-(1-methylpyridinium)vinyl]-bis(9-methyl-carbazol-3-yl)-methane diiodide (**I**). As shown in Scheme 1, the molecule contains two vinylpyridinium carbazole moieties connected by a methylene group. Firstly, the non-conjugated structure will keep the photophysical properties of monocyanine, voiding the hyperchromism in UV and bathochromism in fluorescence, resulting in the large Stokes shift. Secondly, the intramolecular charge transfer through the methylene group ("through-space" type) may exist in excited state of the molecule,[35,36] which could dedicate to large TPA cross section. Thirdly, the non-rigid connected bis-cationic centres in the molecule would make it easier to adjust the distance of two cationic centres and the molecular orientation compared with the rigid-connection one in biscyanine, which will cause the strong interaction with DNA. In order to get better understanding of the molecular characteristics, we have investigated the properties of **I** in comparison to monocyanine, 3-[2-(1-methylpyridinium)vinyl]-9-methyl carbazole iodide (**II**) and its biscyanine counterpart, 3,6-bis[2-(1-methylpyridinium)-vinyl]-9-methyl carbazole diiodide (**III**). Aside from studying the interaction between these compounds and DNA, we have further applied them into staining HeLa cells. The capability of molecule **I** to specifically bind to DNA and its low cytotoxicity have been successfully demonstrated. These advantages predict the potential application in selective labelling of HeLa cells by both confocal fluorescence and TPEF microscopy bioimaging.

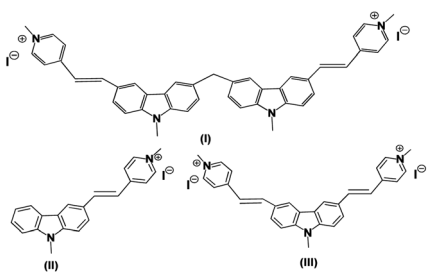


Scheme 1 The chemical structure of carbazole-based cyanine probes.

## Experimental section

### Materials

9*H*-Carbazole, sodium hydride (60% in mineral oil, NaH), trichlorophosphine oxide ($POCl_3$), methyliodine ($CH_3I$), sodium hydroxide (NaOH), 4-methylpyridine and all of the solvents were obtained from Beijing Chemical Reagent Company and used without further purification. Sodium iodide (NaI), chlorotrimethylsilane (TMSCl) and *n*-butyllithium were purchased from Arcos Organics (Belgium). Anhydrous tetrahydrofuran (THF) and Tris–HCl buffer (pH = 7.4) were purchased from HEOWNS (China). MitoTracker Deep Red was purchased from Invitrogen. 3-Bromo-9*H*-carbazole and calf thymus DNA (ct-DNA) were purchased from Sigma Co. (USA).

The concentration of ct-DNA was estimated by measuring the UV absorbance at 260 nm ($\varepsilon$ = 6600 $M^{-1}$ $cm^{-1}$). All of the oligonucleotides were purchased from SBS Genetech Co., Ltd. (Beijing, China), purified by PAGE. All of them were dissolved in 10 mM Tris–HCl buffer solutions containing 100 mM NaCl and 1 mM EDTA. Then DNA samples were heated to 94 °C for 5 min, gently cooled at room temperature, and then stored at 4 °C before use.

### Measurements

$^1$H NMR and $^{13}$C NMR spectra were recorded on a Varian Jemini-300/Brucker AV 400 spectrometer using $CDCl_3$ or DMSO-d6 as a solvent and all shifts are referred to tetramethylsilane (TMS). The chemical shift (s = singlet, d = doublet, t = triplet, and m = multiplet) is shown in ppm. High resolution mass spectra (HRMS) were recorded on a Microflex (Bruker, Germany). The ESI mass spectra were determined on a Q-Tof Mass Spectrometer (Waters). Melting points were measured on an X-4 microscopic melting-point apparatus produced by Beijing Focus Instrument Company.

UV-Vis spectra were recorded at a concentration of $1 \times 10^{-5}$ M on a Hitachi U-3900 spectrophotometer. One-photon excited fluorescence (OPEF) spectra were recorded at a concentration of $2.5 \times 10^{-6}$ M using a Hitachi F-4600 spectrometer. The fluorescence quantum yields were obtained following the

 

expression with fluorescein in 0.1 M NaOH aqueous solution as a reference standard ($\Phi_r = 0.90$) by eqn (1).[37,38]

$$\Phi_s = \Phi_r \left[\frac{A_r(\lambda_r)}{A_s(\lambda_s)}\right]\left[\frac{I_r(\lambda_r)}{I_s(\lambda_s)}\right]\left[\frac{n_s}{n_r}\right]^2\left[\frac{F_s}{F_r}\right] \quad (1)$$

where $\Phi$ is the quantum yield, $n$ is the refractive index, $I(\lambda)$ is the relative intensity of exciting light at wavelength $\lambda$, $A(\lambda)$ is the absorbance of solution at the exciting wavelength $\lambda$, and $F$ is the integrated area under the emission spectrum. Subscripts s and r refer to the sample and reference solution, respectively.

TPEF spectra were recorded using a SD2000 spectrometer (Ocean Optics), excited by a femtosecond laser (Mai Tai, Spectra-Physics, Fremont, CA) with a pulse width of 100 fs and a repetition rate of 80 MHz. TPA cross-sections were determined by the TPEF method.[39] It is assumed that the quantum efficiencies after two-photon excitation are the same as those after one-photon excitation. The TPA cross-sections were obtained by calibration against fluorescein with a known $\Phi\delta$ value in NaOH aqueous solution (pH = 11) at a concentration of $1.0 \times 10^{-4}$ M. The samples were dissolved in solvents at a concentration of $1.0 \times 10^{-4}$ M. The error of TPEF measurement is about 15%. To ensure that the measured signals were solely due to TPA, the dependence of TPEF on the incident intensity was verified in each case to be quadratic (Fig. S1†). Then the TPA cross-sections were calculated according to eqn (2):

$$\delta_s = \delta_r \frac{C_r}{C_s}\frac{n_r}{n_s}\frac{F_s}{F_r}\frac{\Phi_r}{\Phi_s} \quad (2)$$

where $\delta$ is the TPA cross-section, $C$ and $n$ are the concentration and refractive index of the sample solution, and $F$ is the integrated area obtained from the TPEF spectrum.

### Circular dichroism spectroscopy

The circular dichroism (CD) spectra were recorded from both DNA and compounds absorbing region on a Jasco J-815 spectrometer in a 1 cm quartz cuvette thermostat at 20 °C. 220 nm is the lowest wavelength achievable, because Tris–HCl absorbs strongly below 220 nm, leading to a rise of the photomultiplier voltage and unreliable results.[40] Each spectrum was the accumulation of four scans at a scanning speed of 200 nm $min^{-1}$, with a response time of 0.125 s, 0.5 nm pitch and 1 nm bandwidth. The probes with concentration ranging from 0 to 25 μM were titrated into 5 μM solutions of DNA. Each CD spectrum was taken after 10 min incubation.

### Cell culture and fluorescence images

HeLa cells were cultured in culture media (DMEM–F12 1 : 1 (HyClone) with 10% Fetal Bovine Serum (FBS) and 1% penicillin–streptomycin) at 37 °C under a humidified atmosphere containing 5% $CO_2$ for 24 h. The sample was prepared using the glass-bottom cuvette (NEST). Precooled 99% methanol (−20 °C) was used to fix cells for 1.5 min, subsequently the methanol was removed and the cells were washed with PBS twice. Then the pretreated HeLa cells were stained with the 1.5 μM probe for 15 min at room temperature. Cells were rinsed with PBS twice and ready for confocal fluorescence microscopy observation.

The cell viability was tested using MTT (3-(4,5-dimethylthiazol-2-yl)-2,5-diphenyltetrazolium bromide) assay, which is based on the mitochondrial conversion of tetrazolium salt. The HeLa cells were seeded in 96-well microplates (Costar, Corning, NY) at a density of $1.0 \times 10^4$ cells per well in 100 μL DMEM medium. After attachment for 24 h, the cells were incubated with probes at various concentrations for another 24 h in a final volume containing 150 μL medium, and then the medium was removed. After that, 150 μL of fresh medium and 10 μL of MTT (5 mg $mL^{-1}$ in PBS) were added to each well, and the culture plates were incubated at 37 °C and 5% $CO_2$ for 4 h. After removing the medium, 150 μL of dimethyl sulfoxide (DMSO) was added to each well to dissolve the dye. The absorbance at 492 nm was measured using a microplate reader. Each data point was derived from three parallel samples.

Confocal fluorescence imaging was performed with a Nikon multiphoton microscope (A1R MP) with a 60× oil-immersion objective lens and living cell workstation. Confocal fluorescence images were obtained with an excitation of 488 nm (coherent). TPEF imaging was excited at 820 nm using a femtosecond laser (Mai Tai, Spectra-Physics).

### Synthetic procedures

As shown in Scheme 2, compound **I** was synthesized in a facile way.[41,42] Compounds **II** and **III** were synthesized according to the literature.[43–45]

**Synthesis of bis(9-methyl-carbazol-3-yl)methanol (A).** In a 100 mL flask, a solution of 3-bromo-*N*-methyl-carbazole (2.63 mmol, 683 mg) in anhydrous THF (30 mL) was stirred and cooled at −80 °C under a nitrogen atmosphere. A solution of *n*-butyllithium (3.75 mmol, 1.5 mL) in hexane (2.5 M) was slowly added to the solution and stirred for 30 min. Then a suspension of 9-methylcarbazolyl-3-aldehyde (2.60 mmol, 545 mg) in 20 mL anhydrous THF was added. After one hour, the cooling bath was removed and stirred overnight. The reaction mixture was quenched by adding 30 mL water and extracted with dichloromethane. The solvent was removed under vacuum. After recrystallization using dichloromethane, **A** was obtained as a white solid (789 mg, 78% yield). $^1$H NMR (400 MHz, $CDCl_3$, ppm): 2.35 (d, 1H, $J = 3.6$ Hz), 3.85 (s, 6H), 6.30 (d, 1H, $J = 3.6$ Hz), 7.20 (t, 2H, $J = 3.6$ Hz), 7.37 (t, 2H, $J = 7.2$ Hz), 7.52 (d, 2H, $J = 8.4$ Hz), 8.07 (d, 2H, $J = 7.6$ Hz), 8.21 (s, 2H). HR-MS ($C_{27}H_{22}N_2O$): calcd: 390.1732; found: 390.1721.

**Synthesis of bis(9-methyl-carbazol-3-yl)methane (B).** In a 100 mL flask, a solution of NaI (2.00 mmol, 320 mg) and

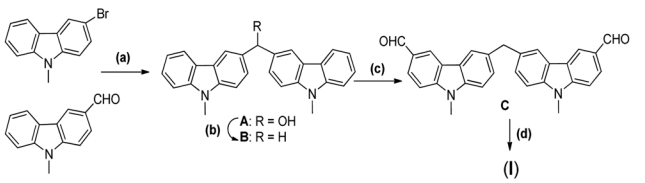


Scheme 2 Synthesis route of the new cyanine. Reagents and conditions: (a) *n*-butyllithium, anhydrous THF, −80 °C to RT, $N_2$; (b) TMSCl, NaI, $CH_3CN$, RT; (c) $POCl_3$/DMF, $ClCH_2CH_2Cl$, reflux; (d) 1,4-dimethylpyridinium iodide, piperidine (catalytic amount), ethanol, reflux.

chlorotrimethylsilane (TMSCl) (2.00 mmol, 0.2 mL) in $CH_3CN$ (15 mL) was stirred at 0 °C in an ice-water bath under a $N_2$ atmosphere. A solution of **A** (0.50 mmol, 200 mg) in $CH_3CN$ (10 mL) was added dropwise to maintain the reaction temperature below 0 °C. The reaction mixture was allowed to warm to room temperature overnight (12 h) and was recooled to 5 °C before use. A solution of NaOH (60 mg with 30 mL $H_2O$) was added over 10 min. The reaction mixture was extracted with ethyl acetate (3 × 25 mL). The organic phase was dried over anhydrous $MgSO_4$ and rotary evaporated to give a viscous liquid, which was purified by silica gel column chromatography, elution of the column with an ethyl acetate and petroleum ether mixture (1 : 20) gave white powder **B** (95 mg, 51% yield). $^1$H NMR (400 MHz, $CDCl_3$, ppm): 3.83 (s, 6H), 4.37 (s, 2H), 7.18 (t, 2H, $J$ = 7.6 Hz), 7.31–7.38 (m, 6H), 7.45 (t, 2H, $J$ = 8.4 Hz), 7.97 (s, 2H), 8.01 (d, 2H, $J$ = 7.6 Hz). HR-MS ($C_{27}H_{22}N_2$): calcd: 374.1783; found: 374.1745.

**Synthesis of 6,6′-methylenebis(9-methyl-carbazole-3-carbaldehyde) (C).** To a 250 mL three-necked flask containing DMF (1.5 mL, 15 mmol) in an ice-water bath, trichlorophosphine oxide (2.5 mL, 15 mmol) was added dropwise; half an hour, a solution of **B** (3.00 mmol, 1.12 g) in 1,2-dichloroethane (10 mL) was added dropwise. The resulting mixture was allowed to reflux for 24 h at 90 °C under a $N_2$ atmosphere. The resulting suspension was carefully poured into ice water and then neutralized by saturated NaOH solution to slightly tune the alkalinity and then extracted with $CH_2Cl_2$ (3 × 100 mL). The organic phase was dried over anhydrous $MgSO_4$ and rotary evaporated to give a viscous liquid, which was purified by silica gel column chromatography, elution of the column with the ethyl acetate and petroleum ether mixture (1 : 3) gave light yellow powder **C** (0.38 g, 30%). $^1$H NMR (400 MHz, $CDCl_3$, ppm): 3.90 (s, 6H), 4.40 (s, 2H), 7.39 (d, 2H, $J$ = 8.4 Hz), 7.45 (d, 2H, $J$ = 8.4 Hz), 7.99 (s, 2H), 8.01 (d, 2H, $J$ = 6.4 Hz), 8.55 (s, 2H), 10.05 (s, 2H). HR-MS ($C_{29}H_{22}N_2O_2$): calcd: 430.1681; found: 430.1650.

**Synthesis of 6,6′-bis[2-(1-methylpyridinium)vinyl]-bis(9-methyl-carbazol-3-yl)methane diiodide (I).** To a 100 mL flask containing 1,4-dimethyl-pyridiniumiodide (10 mmol) and **C** (4 mmol) in ethanol (30 mL), piperidine (catalytic amount) was added dropwise. The resulting mixture was allowed to reflux for 48 h. After filtration and recrystallization using methanol, **I** was obtained as reddish-yellow solids. Yield: 51.3%. Mp > 290 °C. $^1$H NMR (400 MHz, DMSO-d6, ppm): 3.91 (s, 6H), 4.22 (s, 6H), 4.37 (s, 2H), 7.48–7.53 (m, 4H), 7.60 (d, 2H, $J$ = 8.4 Hz), 7.71 (d, 2H, $J$ = 8.4 Hz), 7.86 (d, 2H, $J$ = 7.6 Hz), 8.07 (s, 2H), 8.07–8.19 (m, 8H), 8.53 (s, 2H), 8.77 (d, 2H, $J$ = 7.2 Hz). $^{13}$C NMR (400 MHz, DMSO-d6, ppm): 29.3, 40.8, 47.3, 110.3, 110.5, 120.4, 120.8, 121.6, 122.1, 123.3, 126.8, 127.0, 134.3, 140.5, 142.8, 142.9, 145.3, 153.7. MS (ESI): $m/z$ calcd: for $C_{43}H_{38}I_2N_4$ 305.4 $[M - 2I]^{2+}$; found: 305.4.

**3-[2-(1-Methylpyridinium)vinyl]-9-methyl-carbazole iodide (II) and 3,6-bis[2-(1-methylpyridinium)vinyl]-9-methyl-carbazole diiodide (III).** 3-[2-(1-Methylpyridinium)vinyl]-9-methyl-carbazole iodide (**II**) and 3,6-bis[2-(1-methylpyridinium)vinyl]-9-methyl-carbazole diiodide (**III**) were also obtained by a similar procedure as described for **I**.

*Compound **II**.* Yield: 60.3%. Mp > 290 °C. $^1$H NMR (400 MHz, DMSO-d6, ppm): 3.94 (s, 3H), 4.24 (s, 3H), 7.30 (t, 1H, $J$ = 7.6 Hz), 7.50–7.56 (m, 2H), 7.66 (d, 1H, $J$ = 8.4 Hz), 7.73 (d, 1H, $J$ = 8.8 Hz), 7.91 (d, 1H, $J$ = 8.4 Hz), 8.17–8.23 (m, 4H), 8.58 (s, 1H), 8.80 (d, 2H, $J$ = 6.4 Hz). $^{13}$C NMR (400 MHz, DMSO-d6, ppm): 30.6, 48.1, 111.2, 111.4, 121.1, 121.4, 121.7, 122.5, 123.3, 123.9, 124.2, 127.6, 127.9, 142.8, 143.4, 143.8, 146.2, 154.5. MS (ESI): $m/z$ calcd: for $C_{21}H_{29}IN_2$ 299.2 $[M - I]^+$; found: 299.1.

*Compound **III**.* Yield: 48.8%. Mp > 290 °C. $^1$H NMR (400 MHz, DMSO-d6, ppm): 3.99 (s, 3H), 4.26 (s, 6H), 7.56 (s, 1H), 7.60 (s, 1H), 7.79 (d, 2H, $J$ = 8.4 Hz), 7.98 (d, 2H, $J$ = 8.4 Hz), 8.21–8.26 (m, 6H), 8.64 (s, 2H), 8.83 (d, 4H, $J$ = 6.8 Hz). $^{13}$C NMR (400 MHz, DMSO-d6, ppm): 29.5, 46.7, 110.5, 120.5, 121.1, 122.5, 122.8, 126.6, 127.0, 141.9, 142.4, 144.8, 152.8. MS (ESI): $m/z$ calcd: for $C_{29}H_{27}I_2N_3$ 208.6 $[M - 2I]^{2+}$; found: 208.7.

## Results and discussion

### Synthesis

Diarylmethane can be synthesized using Friedel–Craft reaction.[46] We failed in synthesizing the intermediate **B**, bis(9-methyl-carbazol-3-yl)methane, *via* a direct Friedel–Craft reaction between carbazole and chloromethylcarbazole derivatives due to the polymerization of halomethyl carbazole derivatives under acidic conditions.[47] The carbazolylation afforded the bis(9-methylcarbazol-3-yl)methane core *via* tandem Grignard reaction and iodo-trimethylsilane (TMSI) mediated reduction encouraged us.[42] Starting from 3-bromo-9-methylcarbazole and 9-methylcarbazolyl-3-aldehyde, compound **A** was obtained by 9-methylcarbazole carbonylation with 78% yield after recrystallization in dichloromethane. A further reduction reaction of **A** with TMSI provided **B** in 53% yield after column chromatography. Finally, compound **C**, synthesized by Vilsmeier–Haack reaction,[48] was reacted with *N*-methyl-4-methyl-pyridium iodide and converted into **I** in moderate yield by the Knoevenagel reaction according to the literature.[43–45] Compounds **II** and **III** were synthesized in a similar way.

### One- and two-photon photophysical properties

The normalized one-photon absorption and fluorescence spectra in DMSO of **I, II, and III** are shown in Fig. 1a. The absorption spectral shapes of **I** and **II** are extremely similar. Unlike them, **III** shows a lowest excited band at 445 nm and the second excited band at 403 nm, attributed to the coupling of two ICT branches. The increased vinylpyridinium carbazole moiety in **I** leads to the twice higher extinction coefficients ($\varepsilon$) in comparison to **II**. The absorption and emission maximum of **I** show 7 nm and 11 nm red shifts in relative to those of **II**, respectively (Table 1). We suppose that the red shift phenomena of **I** mainly result from the two branched components similar to **II** *via* "through-space" charge transfer.[35]

Keeping this in mind, we further investigated the TPA properties of the compounds. Glycol was used as a viscous solvent to improve the fluorescence quantum yields in order to reduce the error of TPA cross-sections caused by the quantum efficiency. **I** exhibits a maximum at 591 nm in TPEF spectra when excited at 820 nm in glycol. The TPEF spectra are in accordance with the OPEF spectra (Fig. S2†). Using the TPEF method, TPA spectra were obtained as shown in Fig. 1b. The

 

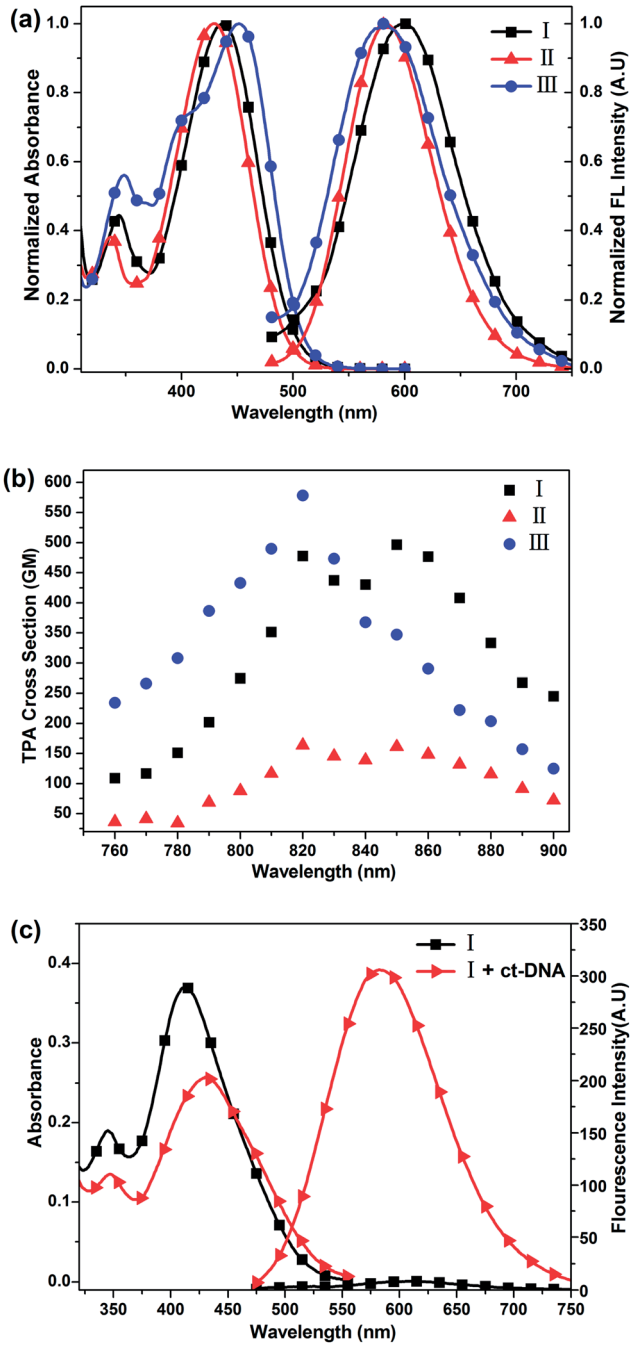


Fig. 1 (a) Normalized absorption and one-photon induced fluorescence spectra of I, II and III in DMSO; (b) TPA spectra of I, II and III in the wavelength range of 760 to 900 nm in glycol. (c) Absorption spectra and fluorescence spectra of I ($1 \times 10^{-5}$ M) without and with 5 equiv. of calf thymus DNA (ct-DNA) in Tris–HCl buffer.

large $\delta_{max}$ of **III** (578 GM) is in good agreement with the absorption spectrum, which is assigned to the second ICT state from the strong interaction between two branched vinyl groups. Obviously, TPA spectra of **I** and **II** are also very similar and consistent with their one-photon absorption spectra. The maximum TPA cross-section ($\delta_{max}$) of **I** is 497 GM, about 3 times larger than that of **II** (161 GM). Therefore, the non-rigid connection cannot simply be described as two non-interacting monocyanine groups. We believe that the effective through-space interaction between carbazole-based monocyanine moieties through the methylene group contributes to the TPA enhancement of **I** compared to **II**.[49] The enhanced TPA cross-section implies the potential of **I** for TPEF imaging applications.

Moreover, we noticed that compound **I** is highly sensitive to the micro-environment. In the Tris–HCl buffer solution, the absorption maximum of **I** was blue shifted to 414 nm with an extinction coefficient reduced to $4.03 \times 10^4$ $M^{-1}$ $cm^{-1}$, which was only 20% larger than that of **II**. Meanwhile, when 5 equiv. of ct-DNA was added to the buffer solution, the absorption maximum of **I** was red shifted to 430 nm and the extinction coefficient was reduced to $2.67 \times 10^4$ $M^{-1}$ $cm^{-1}$. When excited at $\lambda_{max}^{abs}$, these compounds showed a weak emission in Tris–HCl buffer while the fluorescence quantum yield increased significantly in organic solvents. The emission maximum of **I** in Tris–HCl buffer appeared at 615 nm with 201 nm Stokes shift, which was 39 nm larger than that of **II**, indicating that the excited state arising from the through-space charge transfer was highly stabilized by the aqueous medium (Fig. S3†). It is important to note that the fluorescence signal of **I** was too low to be calculated accurately ($\Phi_{FL} < 0.001$) in the buffer alone, but more than 30-fold enhancement was observed at saturation with low ct-DNA concentration (5 equiv.). The fluorescence enhancement can be attributed to the restricted intramolecular rotation of **I** after binding with DNA, which would cause the reduction of the nonradiative decay. The significant decrease of extinction coefficient and dramatic increase of fluorescence intensity with the existence of DNA in buffer solution (Fig. 1c) indicate that **I** is expected to interact with DNA and immobilize inside DNA. The result highlights that **I** is of high potential as an excellent fluorescence light-up red probe for DNA at a low concentration.

### Determining the binding mode by circular dichroism titration

The enhanced fluorescence intensity of probes in DNA can be attributed to the micro-environment change or the interaction with DNA, thus we further studied the CD spectra to verify the probe–DNA interactions using different sequences of DNA. Previous work has shown that carbazole dication derivatives can interact with both AT and GC sequences of DNA, and especially prefer to bind towards AT-rich regions.[50] It has also been shown that bisvinylpyridinium carbazole derivatives can stabilize the G-quadruplex DNA structure in human telomeres.[51] CD spectra of DNA and induced CD (ICD) spectra of ligands can be employed to characterize the structure and dynamics of DNA–ligand complexes.[52,53] The CD spectral profile (Fig. S4†) of oligonucleotides (Table 2) we used in Tris–HCl buffer with $Na^+$ confirmed the parallel quadruplex of c-kit2 (ref. 54) with a positive band around 260 nm and a negative band around 240 nm, antiparallel quadruplex of HUM24 with two positive bands at 245 nm and 290 nm and a negative band at 265 nm, and the same B-DNA structure of LD and Drew AT with a positive band at 280 nm and a negative band at 255 nm.[55]

As the binding mode plays an important role in illustrating the interaction of DNA and probe molecules, we performed the CD titration to determine the binding mode of the probe–DNA

Table 1 Optical properties of cyanines at room temperature

| | Solvent | $\lambda_{abs}$[a]/nm | $\varepsilon$[b]/$\times 10^4$ $M^{-1}$ $cm^{-1}$ | $\lambda_{em}$[c]/nm | $\lambda_{em}$[d]/nm | ST[e]/nm | $\varphi$[f] | $\delta$[g]/GM |
|---|---|---|---|---|---|---|---|---|
| **I** | Glycol | 442 | 5.96 | 588 | 591 | 146 | 0.011 | 497 |
| | DMSO | 437 | 5.80 | 596 | — | 159 | 0.005 | — |
| | Tris–HCl buffer | 414 | 4.03 | 615 | — | 201 | <0.001 | — |
| | With ct-DNA[h] | 430 | 2.67 | 585 | — | 155 | 0.024 | — |
| **II** | Glycol | 434 | 3.12 | 577 | 576 | 143 | 0.127 | 161 |
| | DMSO | 430 | 2.90 | 585 | — | 155 | 0.113 | — |
| | Tris–HCl buffer | 418 | 3.21 | 580 | — | 162 | 0.015 | — |
| | With ct-DNA[h] | 446 | 2.52 | 570 | — | 114 | 0.123 | — |
| **III** | Glycol | 455 | 5.30 | 571 | 570 | 116 | 0.023 | 578 |
| | DMSO | 452 | 5.13 | 582 | — | 130 | 0.016 | — |
| | Tris–HCl buffer | 445 | 4.43 | 555 | — | 110 | 0.005 | — |
| | With ct-DNA[h] | 465 | 4.28 | 572 | — | 107 | 0.037 | — |

[a] The wavelength of absorption maximum. [b] The extinction coefficient. [c] The wavelength of one-photon emission maximum. [d] The wavelength of two-photon emission maximum. [e] Stokes shift. [f] Fluorescence quantum yield. [g] The maximum TPA cross measured by the TPEF method (1 GM = $10^{-50}$ $cm^4$ s per photon). [h] 5 equiv. of ct-DNA was added.

Table 2 Oligonucleotides used in this study

| | Sequence (5′–3′) | Structure |
|---|---|---|
| LD | GCGCAATTGCGC | Duplex |
| Drew AT | CGCGAAATTTCGCG | Duplex |
| HUM24 | TTAGGGTTAGGGTTAGGGTTAGGG | Quadruplex |
| c-kit2 | GGGCGGGCGCGAGGGAGGGG | Quadruplex |

interaction. Although this class of compounds shows significant fluorescence enhancement when binding with various oligonucleotides,[30,31] CD spectra show more detailed difference in binding properties. In the presence of **I** in LD and Drew AT, increased positive CD signals at 358 nm and 437 nm were induced along with the increase of probe concentration (Fig. 2a and b). The phenomenon provides strong evidence of groove binding mode as groove complex formation generally exhibits a strong ICD signal.[56] In general, the groove binder prefers to bind within the minor groove in the AT riched region for the larger negative electrostatic potentials and the steric hindrance caused by guanine.[57] Large ICD signals were also observed in the case of **III** within the absorption region of the probe, which had been proved as a minor-groove binder to duplex DNA (Fig. S5†). The results provide further evidence that molecule **I** can insert into the minor-groove in the central AT region of the two duplex DNA.[58] In addition, an excitonic ICD signal showing a split negative couplet band (500 nm for **I** and 420 nm for **III**) was observed as a result of the interaction between molecules outside DNA and their adjacent bound ones in the minor groove. In contrast, **II** did not exhibit obvious ICD signals when interacted with LD and Drew AT (Fig. S6†), indicating the intercalation binding mode and weak binding strength.[28]

The interaction between G-quadruplex and ligands is complex because there are several binding sites in diverse types of quadruplex structures. Previous work has proved that the analogs of **III** show a strong ICD signal when binding to a telomeric G-quadruplex.[59] In our study, we also observed a similar result in HUM24, one of the human telomeric DNA (Fig. S5†). It can be dominated by its binding preference to the end of G-quartet with the diagonal loop. As for c-kit2 with a parallel structure, the ICD signal was not observed even at a high probe–DNA ratio. The reason may lie in the absence of the diagonal loop in parallel type G-quadruplex.[60] Interestingly, obvious ICD signals were induced in the absorption region of **I** when interacted with both HUM24 and c-kit2. The quite different ICD patterns when **I** and **III** interacted with HUM24 could be attributed to the different binding modes. It is likely that the binding mode of **I** to G-quadruplex is external stacking on the end surface of the G-quartet or groove binding. Moreover, Fig. 2c and d show similar ICD patterns characterized by a positive and a negative band of **I** in HUM24 and c-kit2. But the difference in peak location implies that groove binding is likely to be the major binding mode as the ICD signals are perturbed by different quadruplex structures.[61] However, the induced CD signals of **II** in quadruplex are also negligible, indicating that the methylene bridge in **I** adjusts the molecule's configuration and orientation easily to fit the binding sites of DNA. Although the detailed binding preference deserves further investigation, it is clear that this symmetric molecule (**I**) with bis-cationic centres provided by two non-rigid connected carbazole-based monocyanines can effectively interact with various DNA structures.

## Confocal fluorescence and TPEF microscopy imaging

Based on the understanding of the interaction with DNA, the probe with fluorescence enhancement would be prospective for cell imaging. The cytotoxicity of the organic molecular probes is an important issue for living organelle staining. We performed the MTT assay to examine the cytotoxic behavior of the three probes. HeLa cell viability was assessed 24 h after incubating with different concentrations of probes. Control experiments were conducted in a similar manner without the presence of the probes. As shown in Fig. 3a, the viability of HeLa cells was over 80% even at 100 μM of **I**. However, the analogues of previously

 

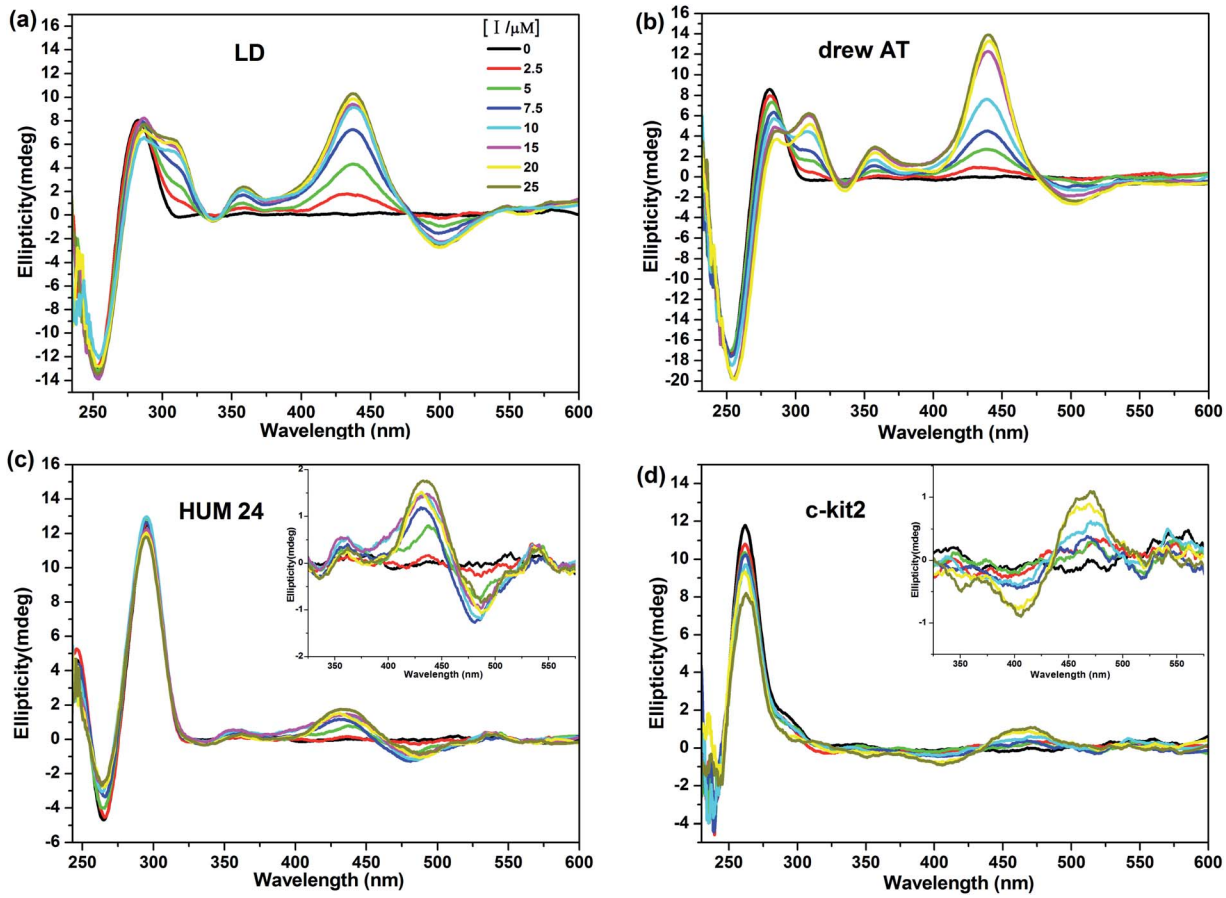


Fig. 2 Circular dichroism spectra of 5 μM (a) LD, (b) Drew AT, (c) HUM24 and (d) c-kit2 upon titration of **I** (0–25 μM) in 10 mM Tris–HCl buffer containing 100 mM NaCl and 1 mM EDTA. The insets in (c) and (d) show the corresponding induced CD spectra during titration.

reported carbazole-based cyanines **II** and **III** exhibited obvious cytotoxicity at high concentration, of which the IC-50 values were 26.3 μM and 47.8 μM, respectively. The low cytotoxicity of probe **I** enables it to make a trade-off between visibility and cytotoxicity easily for fluorescence imaging.

Fluorescence microscopy is a powerful tool to monitor and visualize the intracellular distribution of probes. Confocal microscopy imaging study of these probes in living HeLa cells was carried out to investigate the staining selectivity. The excitation wavelength was 488 nm and the emission was collected in a range of 570–620 nm. Previous work about the characteristics of 1D and 2D carbazole-based cyanines imaged in HeLa cells showed that molecules with a short alkyl chain ($CH_3$) on the carbazole nitrogen were directed to both mitochondria and nucleus.[62] Our observations are mostly consistent with the result that probes **II** and **III** are distributed on both cytoplasm and nucleus without specific staining selectivity to a single subcellular structure (Fig. S7†). In contrast, probe **I** exhibited specific localization in cell cytoplasm with high selectivity (Fig. 3b). Further analysis of the staining dynamics in living cells also demonstrated that **I** could penetrate the cell membrane directly and accumulate in the cytoplasm region specifically with continuously increasing fluorescence intensity (Fig. S7†). To determine the cellular localization of the probe, we performed a co-localization experiment with MitoTracker Deep Red. The resulting images (Fig. S8†) confirmed that probe **I** accumulated mainly in mitochondria. An explanation for that is cationic fluorescent probes, such as rhodamine 123, can always locate to mitochondrial regions because they might be attracted by the relatively high negative electric potential across the mitochondrial membrane.[63] Note that the large molecular dimension and the chromophore shape of **I** limit its karyotheca permeability, which results in the high staining selectivity for mitochondria in a living cell. We further applied **I** to stain fixed cells. The fluorescence intensity was significantly enhanced when **I** entered into nucleus. The image exhibits a high contrast nuclear staining with a low cytoplasmic background (Fig. 3c). The result clearly illustrates that probe **I** can interact efficiently with the nuclear DNA, although further molecule modification is needed to achieve karyotheca permeability in a living cell.

Furthermore, the performance of TPEF imaging with this newly designed probe **I** has been further investigated considering its large TPA cross-section and the significant fluorescence enhancement in subcellular targets. The excitation wavelength was 820 nm. TPEF images exhibited good brightness and excellent contrast even though the observations were performed without removing the fluorescent probe in the surrounding medium (Fig. 4a–c). The result demonstrates that

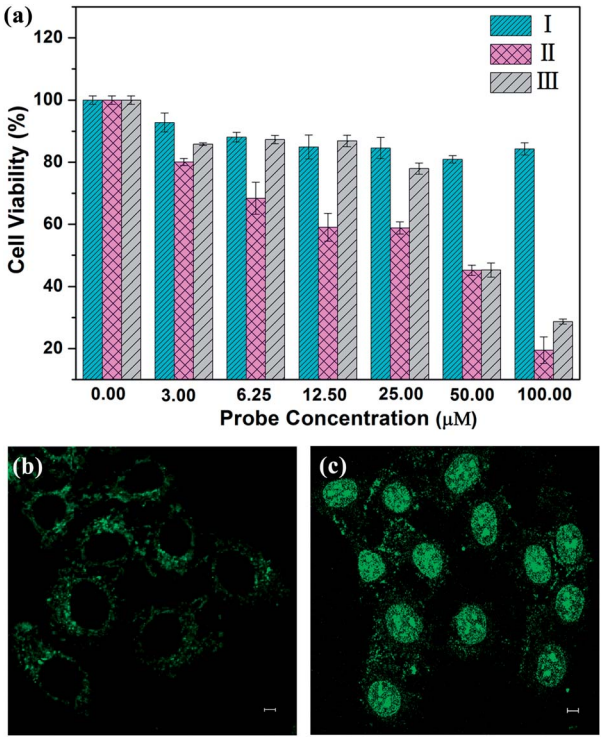


Fig. 3 (a) Cell viability of HeLa cells after incubating with probes of increasing concentrations, as determined by the MTT test. Confocal fluorescence images ($\lambda_{exc}$ = 488 nm) obtained following incubations of (b) living HeLa cells with **I** (3 μM) for 2 h and (c) fixed HeLa cells with **I** (1.5 μM) for 15 min. Scale bar is 5 μm.

the TPEF intensity was significantly enhanced when the probe bounded with the subcellular targets. The 3D optical section of HeLa cells (Fig. 4d) proves that the intrinsic 3D resolution and increased cell penetration depth can be well achieved using **I** as a TPEF probe. The staining selectivity and high brightness of TPEF images demonstrate the potential of **I** for further application in biophotonics and medical science.

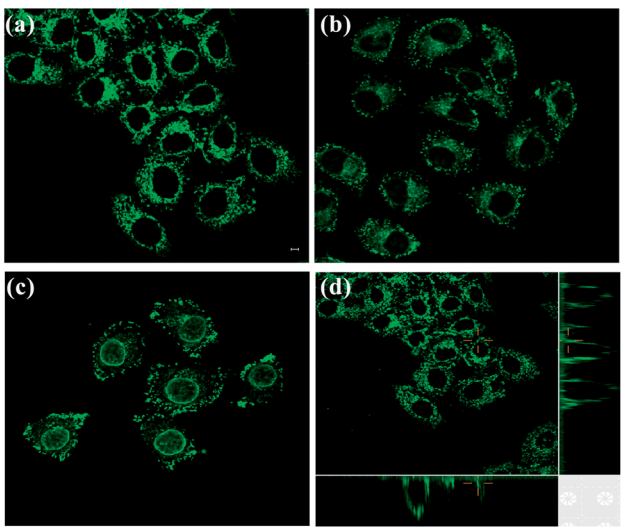


Fig. 4 Two-photon excited ($\lambda_{exc}$ = 820 nm) fluorescence images obtained following incubations of HeLa cells with (a) **I**, (b) **II** and (c) **III** with a concentration of 3 μM for 2 h. (d) 3D TPEF images of HeLa cells incubated with **I**. The penetration depths are 11.5 μm. Scale bar is 5 μm.

## Conclusions

In conclusion, we have designed and synthesized a novel bis-carbazolylmethane-based cyanine, 6,6′-bis[2-(1-methyl-pyridinium)vinyl]-bis(9-methyl-carbazol-3-yl)methane diiodide (**I**), as a TPEF probe for DNA and living cell imaging. The molecule was designed by connecting two vinylpyridinium carbazole moieties with a non-rigid methylene bridge. The optical properties of **I** were successfully demonstrated. The 201 nm Stokes shift in buffer solution and 3-fold enhancement of the TPA cross-section compared to that of the monocyanine **II** are mainly attributed to the "through-space" type intramolecular charge transfer through two vinylpyridinium carbazole groups. This new probe exhibits very weak emission and 30-fold fluorescence enhancement when binding with ct-DNA, giving promise as a fluorescence light-up probe for DNA. The obvious ICD signals in CD spectra proved that molecule **I** with soft-connected bis-cationic centres can specifically interact with various DNA structures by distinctive binding mode. Cell viability study shows that the probe has a very low cytotoxicity. The application of **I** for confocal fluorescence microscopy imaging exhibits high staining selectivity for mitochondria in living HeLa cells. Its capability to stain nuclear DNA was confirmed by fixed cell staining. Furthermore, the properties of the large TPA cross-section and significant fluorescence enhancement in subcellular targets enable **I** to become a highly sensitive TPEF probe for nonlinear bioimaging with high brightness, contrast and 3D resolution. The successful design of this carbazole-based cyanine provides a new way for developing fluorescent light-up probes for DNA and TPEF cell imaging.

## Acknowledgements

We are grateful to the National Natural Science Foundation of China (Grant no. 61205194, 91123032, and 61275171), the National Basic Research Program of China (2010CB934103), and the International Cooperation Program of MOST (2010DFA01180) for financial support. The authors would like to thank Prof. Dr Wei-qiang Chen for valuable discussion about the molecules' design and synthesis.

## Notes and references

1 H. Kobayashi and P. L. Choyke, *Acc. Chem. Res.*, 2010, **44**, 83–90.
2 G. M. van Dam, G. Themelis, L. M. A. Crane, N. J. Harlaar, R. G. Pleijhuis, W. Kelder, A. Sarantopoulos, J. S. de Jong, H. J. G. Arts, A. G. J. van der Zee, J. Bart, P. S. Low and V. Ntziachristos, *Nat. Med.*, 2011, **17**, 1315–1319.
3 W.-E. Lu, X.-Z. Dong, W.-Q. Chen, Z.-S. Zhao and X.-M. Duan, *J. Mater. Chem.*, 2011, **21**, 5650–5659.
4 C. W. Spangler, *J. Mater. Chem.*, 1999, **9**, 2013–2020.

5 M. Velusamy, J.-Y. Shen, J. T. Lin, Y.-C. Lin, C.-C. Hsieh, C.-H. Lai, C.-W. Lai, M.-L. Ho, Y.-C. Chen, P.-T. Chou and J.-K. Hsiao, *Adv. Funct. Mater.*, 2009, **19**, 2388–2397.
6 M. D. Cahalan, I. Parker, S. H. Wei and M. J. Miller, *Nat. Rev. Immunol.*, 2002, **2**, 872–880.
7 W. Denk, J. Strickler and W. Webb, *Science*, 1990, **248**, 73–76.
8 C. Xu, W. Zipfel, J. B. Shear, R. M. Williams and W. W. Webb, *Proc. Natl. Acad. Sci. U. S. A.*, 1996, **93**, 10763–10768.
9 M. S. T. Gonçalves, *Chem. Rev.*, 2008, **109**, 190–212.
10 J. Chan, S. C. Dodani and C. J. Chang, *Nat. Chem.*, 2012, **4**, 973–984.
11 R. W. Sinkeldam, N. J. Greco and Y. Tor, *Chem. Rev.*, 2010, **110**, 2579–2619.
12 T. Jamieson, R. Bakhshi, D. Petrova, R. Pocock, M. Imani and A. M. Seifalian, *Biomaterials*, 2007, **28**, 4717–4732.
13 E. Sharon, R. Freeman and I. Willner, *Anal. Chem.*, 2010, **82**, 7073–7077.
14 C. S. Thaxton, D. G. Georganopoulou and C. A. Mirkin, *Clin. Chim. Acta*, 2006, **363**, 120–126.
15 M.-L. Zheng, K. Fujita, W.-Q. Chen, X.-M. Duan and S. Kawata, *J. Phys. Chem. C*, 2011, **115**, 8988–8993.
16 H. Zhang, J. Fan, J. Wang, S. Zhang, B. Dou and X. Peng, *J. Am. Chem. Soc.*, 2013, **135**, 11663–11669.
17 J. D. Watson and F. H. C. Crick, *Nature*, 1953, **171**, 737–738.
18 L. H. Hurley, *Nat. Rev. Cancer*, 2002, **2**, 188–200.
19 V. P. Tokar, M. Y. Losytskyy, V. B. Kovalska, D. V. Kryvorotenko, A. O. Balanda, V. M. Prokopets, M. P. Galak, I. M. Dmytruk, V. M. Yashchuk and S. M. Yarmoluk, *J. Fluoresc.*, 2006, **16**, 783–791.
20 Z. Li, S. Sun, Z. Yang, S. Zhang, H. Zhang, M. Hu, J. Cao, J. Wang, F. Liu, F. Song, J. Fan and X. Peng, *Biomaterials*, 2013, **34**, 6473–6481.
21 Y. Hong, S. Chen, C. W. T. Leung, J. W. Y. Lam and B. Z. Tang, *Chem. – Asian J.*, 2013, **8**, 1806–1812.
22 M. L. Kopka, C. Yoon, D. Goodsell, P. Pjura and R. E. Dickerson, *Proc. Natl. Acad. Sci. U. S. A.*, 1985, **82**, 1376–1380.
23 M. Read, R. J. Harrison, B. Romagnoli, F. A. Tanious, S. H. Gowan, A. P. Reszka, W. D. Wilson, L. R. Kelland and S. Neidle, *Proc. Natl. Acad. Sci. U. S. A.*, 2001, **98**, 4844–4849.
24 H.-J. Knölker and K. R. Reddy, *Chem. Rev.*, 2002, **102**, 4303–4428.
25 K. Nozaki, K. Takahashi, K. Nakano, T. Hiyama, H.-Z. Tang, M. Fujiki, S. Yamaguchi and K. Tamao, *Angew. Chem., Int. Ed.*, 2003, **115**, 2097–2099.
26 U. Jacquemard, S. Routier, A. Tatibouet, J. Kluza, W. Laine, C. Bal, C. Bailly and J.-Y. Merour, *Org. Biomol. Chem.*, 2004, **2**, 1476–1483.
27 S. Yoon, J.-H. Kim, Y. J. Lee, M. Y. Ahn, G. Choi, W. K. Kim, Z. Yang, H. J. Lee, H. R. Moon and H. S. Kim, *Eur. J. Pharmacol.*, 2012, **697**, 24–31.
28 X. J. Feng, P. L. Wu, F. d. r. Bolze, H. W. C. Leung, K. F. Li, N. K. Mak, D. W. J. Kwong, J.-F. o. Nicoud, K. W. Cheah and M. S. Wong, *Org. Lett.*, 2010, **12**, 2194–2197.
29 M.-L. Zheng, K. Fujita, W.-Q. Chen, N. I. Smith, X.-M. Duan and S. Kawata, *ChemBioChem*, 2011, **12**, 52–55.
30 C.-C. Chang, J.-Y. Wu, C.-W. Chien, W.-S. Wu, H. Liu, C.-C. Kang, L.-J. Yu and T.-C. Chang, *Anal. Chem.*, 2003, **75**, 6177–6183.
31 B. Dumat, G. Bordeau, E. Faurel-Paul, F. Mahuteau-Betzer, N. Saettel, M. Bombled, G. Metgé, F. Charra, C. Fiorini-Debuisschert and M. P. Teulade-Fichou, *Biochimie*, 2011, **93**, 1209–1218.
32 J. Gu, W. Yulan, W.-Q. Chen, X.-Z. Dong, X.-M. Duan and S. Kawata, *New J. Chem.*, 2007, **31**, 63–68.
33 L. Porrès, O. Mongin, C. Katan, M. Charlot, T. Pons, J. Mertz and M. Blanchard-Desce, *Org. Lett.*, 2003, **6**, 47–50.
34 S. Neidle, *Nat. Prod. Rep.*, 2001, **18**, 291–309.
35 J. Zyss, I. Ledoux, S. Volkov, V. Chernyak, S. Mukamel, G. P. Bartholomew and G. C. Bazan, *J. Am. Chem. Soc.*, 2000, **122**, 11956–11962.
36 S. Olsen, *J. Phys. Chem. A*, 2013, **117**, 2455–2468.
37 G. A. Crosby and J. N. Demas, *J. Phys. Chem.*, 1971, **75**, 991–1024.
38 R. Velapoldi and H. Tønnesen, *J. Fluoresc.*, 2004, **14**, 465–472.
39 C. Xu and W. W. Webb, *J. Opt. Soc. Am. B*, 1996, **13**, 481–491.
40 P. Hazel, J. Huppert, S. Balasubramanian and S. Neidle, *J. Am. Chem. Soc.*, 2004, **126**, 16405–16415.
41 E. J. Stoner, D. A. Cothron, M. K. Balmer and B. A. Roden, *Tetrahedron*, 1995, **51**, 11043–11062.
42 J. S. Yadav, D. C. Bhunia, K. Vamshi Krishna and P. Srihari, *Tetrahedron Lett.*, 2007, **48**, 8306–8310.
43 W.-J. Kuo, G.-H. Hsiue and R.-J. Jeng, *Macromolecules*, 2001, **34**, 2373–2384.
44 B. J. Coe, J. A. Harris, I. Asselberghs, K. Clays, G. Olbrechts, A. Persoons, J. T. Hupp, R. C. Johnson, S. J. Coles, M. B. Hursthouse and K. Nakatani, *Adv. Funct. Mater.*, 2002, **12**, 110–116.
45 Y. Zhang, L. Wang, T. Wada and H. Sasabe, *Macromolecules*, 1996, **29**, 1569–1573.
46 C. Borger, M. P. Krahl, M. Gruner, O. Kataeva and H.-J. Knolker, *Org. Biomol. Chem.*, 2012, **10**, 5189–5193.
47 K. Tani, N. Sakumoto, K. Kubono, K. Hori, Y. Tohda, H. Benten, H. Ohkita, S. Ito and M. Yamamoto, *Chem. Lett.*, 2009, **38**, 140–141.
48 A. Vilsmeier and A. Haack, *Ber. Dtsch. Chem. Ges.*, 1927, **60**, 119–122.
49 G. P. Bartholomew, M. Rumi, S. J. K. Pond, J. W. Perry, S. Tretiak and G. C. Bazan, *J. Am. Chem. Soc.*, 2004, **126**, 11529–11542.
50 F. A. Tanious, D. Ding, D. A. Patrick, C. Bailly, R. R. Tidwell and W. D. Wilson, *Biochemistry*, 2000, **39**, 12091–12101.
51 C.-C. Chang, I. C. Kuo, I. F. Ling, C.-T. Chen, H.-C. Chen, P.-J. Lou, J.-J. Lin and T.-C. Chang, *Anal. Chem.*, 2004, **76**, 4490–4494.
52 N. C. Garbett, P. A. Ragazzon and J. B. Chaires, *Nat. Protoc.*, 2007, **2**, 3166–3172.
53 M. Eriksson and B. Nordén, in *Methods in Enzymology*, ed. M. J. W. Jonathan and B. Chaires, Academic Press, 2001, pp. 68–98.
54 V. Kuryavyi, A. T. Phan and D. J. Patel, *Nucleic Acids Res.*, 2010, **38**, 6757–6773.

55 T.-M. Ou, Y.-J. Lu, J.-H. Tan, Z.-S. Huang, K.-Y. Wong and L.-Q. Gu, *ChemMedChem*, 2008, **3**, 690–713.
56 B. Nordén and T. Kurucsev, *J. Mol. Recognit.*, 1994, **7**, 141–155.
57 L. H. Hurley, *J. Med. Chem.*, 1989, **32**, 2027–2033.
58 F. A. Tanious, D. Ding, D. A. Patrick, R. R. Tidwell and W. D. Wilson, *Biochemistry*, 1997, **36**, 15315–15325.
59 J.-Y. Wu, C.-C. Chang, C.-S. Yan, K.-Y. Chen, I. C. Kuo, C.-Y. Mou and T.-C. Chang, *J. Biomol. Struct. Dyn.*, 2003, **21**, 135–140.
60 C.-C. Chang, C.-W. Chien, Y.-H. Lin, C.-C. Kang and T.-C. Chang, *Nucleic Acids Res.*, 2007, **35**, 2846–2860.
61 X.-F. Zhang, H.-J. Zhang, J.-F. Xiang, Q. Li, Q.-F. Yang, Q. Shang, Y.-X. Zhang and Y.-L. Tang, *J. Mol. Struct.*, 2010, **982**, 133–138.
62 E. De Meulenaere, W.-Q. Chen, S. Van Cleuvenbergen, M.-L. Zheng, S. Psilodimitrakopoulos, R. Paesen, J.-M. Taymans, M. Ameloot, J. Vanderleyden, P. Loza-Alvarez, X.-M. Duan and K. Clays, *Chem. Sci.*, 2012, **3**, 984–995.
63 L. V. Johnson, M. L. Walsh and L. B. Chen, *Proc. Natl. Acad. Sci. U. S. A.*, 1980, **77**, 990–994.